Behavior of neutral atoms in a spontaneous force trap

D. W. Sesko, T. G. Walker, and C. E. Wieman

Joint Institute for Laboratory Astrophysics, University of Colorado, and National Institute of Standards and Technology, Boulder, Colorado 80309-0440

Received March 27, 1990; accepted October 10, 1990

A classical collective behavior is observed in the spatial distributions of a cloud of optically trapped neutral atoms. They include extended uniform-density ellipsoids, rings of atoms around a small central ball, and clumps of atoms orbiting a central core. The distributions depend sensitively on the number of atoms and the alignment of the laser beams. Abrupt bistable transitions between different distributions are seen. This system is studied in detail, and much of this behavior can be explained by the incorporation of long-range interactions between the atoms in the equation of equilibrium. It is shown how attenuation and multiple scattering of the incident photons lead to these interactions.

1. INTRODUCTION

Over the past few years rapid progress has been made in the ability to produce large optically trapped samples of cold atoms.[1,2] There have been orders-of-magnitude improvements in the number of atoms trapped and the densities achieved. The deepest optical traps are the Zeeman-shift spontaneous force traps. We have used these to trap 4×10^8 atoms with densities of more than 10^{11} cm^{-3}. At these densities and numbers the gas of cesium atoms becomes optically thick, and forces arising from this optically dense vapor can have a profound effect on the behavior of the cloud. In a recent paper[3] we described a variety of collective effects that arise from this force between the atoms, and we presented a model to explain this behavior. Here we provide more detailed experimental studies and analysis.

The neutral atoms in these traps might naïvely be expected to behave as an ideal gas except when they undergo short-range collisions.[4,5] Although there have been speculations concerning deviations from classical ideal-gas behavior, these centered on Bose–Einstein condensation. This quantum-mechanical phenomenon occurs at temperatures much lower and densities much higher than in the present experiments and is quite different from the behavior discussed here. In this paper we consider collective behavior in which the atomic motion is classical in nature and the behavior is analogous to that observed in plasmas and charged-particle beams. At the densities that we studied, one would not expect such behavior if only conventional interatomic forces between the neutral atoms were involved because the interactions would be dominated by the few nearest neighbors and not involve the cloud as a whole. In this situation the behavior would be much like that of an ideal gas. In contrast, we find that atoms in a spontaneous force trap actually show ideal-gas behavior only for small clouds of atoms. Larger clouds show dramatic dynamic and collective behavior, as Fig. 1 illustrates. We propose that this behavior arises from a strong long-range coupling between the atoms due to the multiple scattering of photons and from the attenuation of the trapping beams as they pass through the cloud. The density and the size of the cloud of atoms are determined by a balance between the above forces and the trapping force. This paper reports on a detailed study of the behavior of optically trapped atoms and the comparison with a theoretical model that includes effects of radiation trapping and the attenuation of the trapping light. In Section 2 we present the theory, in Section 3 we describe the experimental apparatus, and in Section 4 we compare the results of the theoretical calculations with the experimental data.

2. THEORY

A. Growth of Cloud

We consider the force on a trapped atom to be made up of three contributions. The first is the trapping force produced by the laser beams and the Zeeman shifts of the atomic energy levels. The two others are interatomic forces between the trapped atoms. These are the attenuation force, caused by atomic absorption of the laser photons, and the radiation trapping force, arising from the atoms' reradiating the absorbed photons, which are subsequently scattered a second time by other atoms. The first two forces compress the cloud of atoms, while the latter causes it to expand. The three forces are illustrated in Fig. 2 and will be discussed in turn.

The trapping force is a damped-harmonic force and was discussed previously.[1,2] The trap is of the Zeeman-shift spontaneous force type, but the following analysis is suitable for any type of spontaneous force trap forming a damped-harmonic potential. The trapping force can be derived if we consider the force on an atom exerted by three pairs of intersecting circularly polarized beams. Each of these beams is reflected back on itself but with the opposite polarization. We define the polarization of the light with respect to the atoms such that σ^+ (σ^-) polarization drives the $\Delta m = +1$ ($\Delta m = -1$) transitions. These beams intersect at the minimum of a magnetic field of magnitude $B_z = B'_z$. By favoring absorption of one polarization over the other, the magnetic field gradient produces a harmonic potential to first order[2] in each direction such that $\mathbf{F} = -k\mathbf{r}$. The Doppler shift provides a damping that makes the atomic motion overdamped by typically a factor of 10.

0740-3224/91/050946-13$05.00

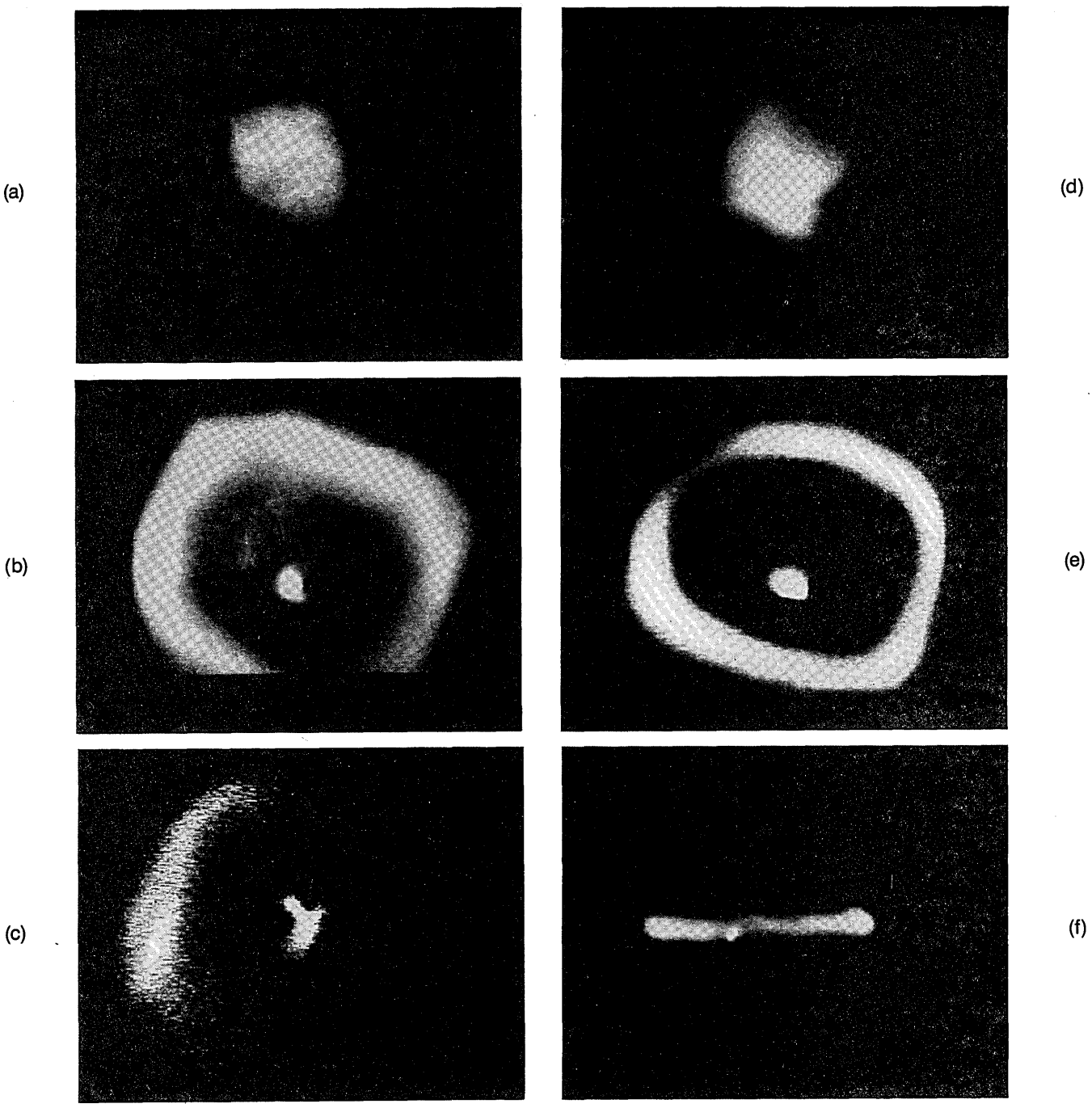

Fig. 1. Spatial distributions of trapped atoms. (a) With fewer than 10^8 atoms, the cloud forms a uniform-density sphere. (b) Top view of rotating clump without strobing. (c) View of (b) with camera strobed at 110 Hz. The clump is rotating around the nucleus in a counterclockwise direction. (d) Top view of rotating clump without strobing but with a smaller radius than in (b) (the clump is one quarter of the area of the total fluorescence). (e) Top view of continuous ring. (f) Side view of (e). The horizontal full scale for (a), (d), (e), and (f) is 1.0 cm. For (b) and (c) it is 0.8 cm.

When many atoms ($>10^4$) are in the trap, the attenuation of the trap laser beams becomes important. The attenuation has three effects. The first is a slight reduction of the spring constant of the trap. Much more important, however, is the force resulting from the local intensity imbalance produced by the absorption, as Figs. 2(a) and 2(c) show. This force was discussed in the context of optical molasses by Dalibard[6] and Kazantsev *et al.*[7] Finally, the intensity of the retroreflected beams is reduced by the first pass through the cloud. This causes an uninteresting shift in the position of the cloud.

The strength of the force associated with the local intensity imbalance is found in the following way. The lasers are initially propagating in opposite directions along the x axis with intensity I_∞ and are attenuated by the trapped atoms. We define an absorption function

$$A_X(\mathbf{r}) = \langle \sigma_L \rangle \int_{-x}^{x} n(\mathbf{r}) \mathrm{d}x, \tag{1}$$

where $\langle \sigma_L \rangle$ is the absorption cross section for the incident laser beams and $n(\mathbf{r})$ is the atomic density of the cloud.

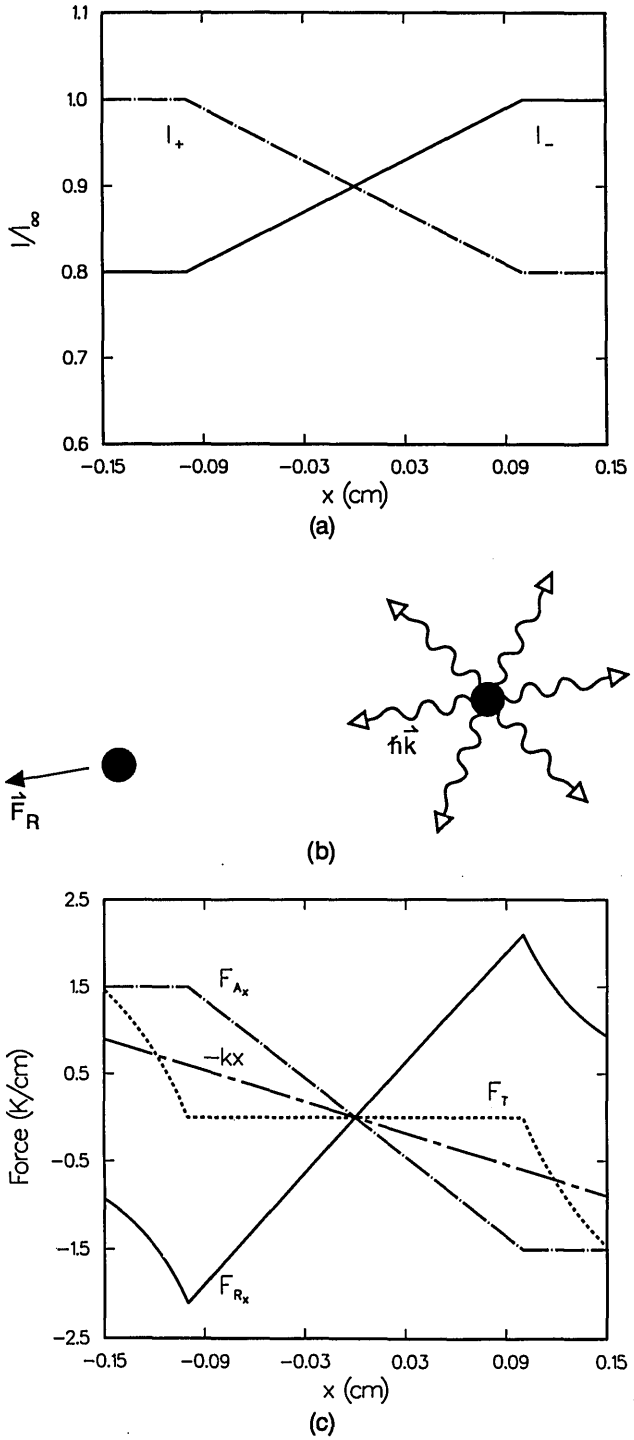

Fig. 2. Forces that arise within an optically thick cloud of atoms. The diameter of the cloud is 0.2 cm. (a) The change in the intensity of the trapping light due to absorption across the cloud of atoms produces the attenuation force $F_{Ax} \propto \langle\sigma_L\rangle(I_+ - I_-)$. (b) The spontaneous emission of two atoms separated by a distance d produces the repulsive radiation trapping force between the atoms, $F_{Rx} \propto \langle\sigma_F\rangle d^{-2}$. (c) The three forces in units of kelvins per centimeter. Note that the total force is $F_T = -kx + F_{Ax} + F_{Rx} = 0$ within the cloud.

Since our maximum absorption of the trapping beams was approximately 20%, we can use the small-absorption approximation (accurate to 2%). Then the spatial dependence of the intensity as a function of x is

$$I_{x_\pm}(\mathbf{r}) = I_\infty\{1 - [A_T(y,z) \pm A_X(\mathbf{r})]/2\}, \tag{2}$$

where A_T is the total absorption of light across the cloud and $I_+(I_-)$ is the intensity of the beam traveling in the positive (negative) coordinate direction. The two unattenuated beams are assumed to have the same intensity I_∞. The force due to the intensity differential between the positive and negative x beams is then

$$F_{A_X}(\mathbf{F}) = -\langle\phi_L\rangle I_\infty A_X(F)/c, \tag{3}$$

where c is the speed of light. By following the same arguments for the y and z directions, we find that the attenuation force $\mathbf{F}_A$ obeys the relation

$$\nabla \cdot \mathbf{F}_A = -6\langle\sigma_L\rangle^2 I_\infty n/c. \tag{4}$$

The negative sign indicates that this attenuation force compresses the cloud or, equivalently, is an effective attractive force between the atoms. This is the force on the atoms due only to the absorption of the trap laser photons.

However, for any real atom these photons must be reemitted, and the re-emitted photons also exert a force. This force is illustrated in Figs. 2(b) and 2(c). It is clear that this must be a repulsive force, because in the process of one atom emitting a photon and a second atom absorbing it, the relative momentum of the atoms is increased by $2\hbar k$. In a laser field of intensity I, an atom absorbs and subsequently reradiates energy at rate $\langle\sigma_L\rangle I$. Thus the intensity of light radiated by one atom at the position of a second atom located a distance d away is

$$I_{\text{rad}} = \langle\sigma_L\rangle I/4\pi d^2. \tag{5}$$

The force on the second atom due to the light emitted by the first is $(I_{\text{rad}}/c)\langle\sigma_F\rangle$, where $\langle\sigma_F\rangle$ is the absorption cross section for the scattered photons. A critical point is that the reradiated light is different from the incident light because of such effects as frequency redistribution and depolarization of the scattered light. Thus the average absorption cross section for the scattered fluorescence light, $\langle\sigma_F\rangle$, is different, in general, from the cross section for the trapping photons, $\langle\sigma_L\rangle$. Using Eq. (5), we obtain a repulsive force between the atoms of magnitude

$$\mathcal{F}_R = \langle\sigma_F\rangle\langle\sigma_L\rangle I/4\pi c d^2. \tag{6}$$

The preceding argument may be extended from two atoms to an arbitrary distribution of atoms, in analogy to Gauss's law of electrostatics, if we assume that an incident photon is unlikely to scatter more than twice. The radiation trapping force thus takes the form

$$\mathbf{F}_R(\mathbf{r}) = \frac{\langle\sigma_F\rangle\langle\sigma_L\rangle I}{4\pi c}\int n(\mathbf{r}')\frac{\mathbf{r}-\mathbf{r}'}{|\mathbf{r}-\mathbf{r}'|^3}\mathrm{d}^3r', \tag{7}$$

and

$$\nabla \cdot \mathbf{F}_R = 6\langle\sigma_F\rangle\langle\sigma_L\rangle I_\infty n(\mathbf{r})/c. \tag{8}$$

Here we have replaced the total average intensity I with the average intensity of each of the six trapping beams, $I_\infty = I/6$, so that Eq. (8) is in the same form as the attenuation force in Eq. (4). Note that the force falls off as $1/r^2$ for an atom outside the cloud distribution just as it does for a point charge outside a charge distribution. To have the same repulsive force as that due to radiation trapping under our conditions, an atom would need a charge of approximately 5×10^{-3} times the charge of the electron.

We may formulate another derivation of the radiation trapping force for a spherical distribution of atoms of uniform density by using the principle of conservation of photons. Here we have that the total outward force on a spherical shell of radius R enclosing N radiating atoms is given by

$$F_R = \langle\sigma_F\rangle I_{\text{rad}}/c, \tag{9}$$

where the total reradiated intensity in a laser field of intensity $I = 6I_\infty$ is

$$I_{\text{rad}} = \langle\sigma_L\rangle IN/4\pi R^2. \tag{10}$$

This result agrees with the solution of Eq. (7) for a spherical cloud of uniform density. It is a good approximation to what we observe for many experimental conditions.

The net force between the atoms due to laser attenuation and radiation trapping can be obtained by adding these two forces. Comparing Eqs. (4) and (8), we see that the net force is repulsive if $\langle\sigma_F\rangle > \langle\sigma_L\rangle$. This condition states that if the cross section for absorption of the reradiated light is greater than that for incident laser light, then the repulsive force due to the re-emission of photons is greater than the attractive force due to the attenuation of the trapping beams. The resulting net repulsive force leads to the expansion of the cloud and thus limits the density of the atoms.

In the limit of zero temperature, if the atoms are in equilibrium the attenuation and radiation trapping forces must balance the trapping force $-k\mathbf{r}$. Empirically, we know that for large clouds the temperature is not greatly important, since the observed value of thermal energy is much less than the trap potential energy ($k_B T \ll kR^2/2$) for a cloud of radius R. If these three forces add to 0, then the divergences of these forces must also add to 0. By adding the divergence of the trapping force, $\nabla\cdot(-k\mathbf{r}) = -3k$, to Eqs. (4) and (8), we arrive at an equation of equilibrium that gives the maximum density of atoms in the cloud,

$$n_{\max} = ck/2\langle\sigma_L\rangle(\langle\sigma_F\rangle - \langle\sigma_L\rangle)I_\infty, \tag{11}$$

for $\langle\sigma_F\rangle > \langle\sigma_L\rangle$. If $\langle\sigma_F\rangle \le \langle\sigma_L\rangle$, then the net force is always compressive and Eq. (11) is invalid. Thus, as atoms are added to the trap, the size of the cloud increases but the density is unchanged.

We can obtain a more general calculation of the atomic distribution by numerically solving the equation of equilibrium in which a pressure gradient is balanced by the trapping and radiation forces. This is somewhat like the equation of hydrostatic equilibrium in stars, with the trapping force having replaced gravity.[8] In our case the pressure gradient across the cloud is $\nabla P = T\nabla n + n\nabla T$. For simplicity, we assume the temperature gradient across the cloud to be negligible, so for the atoms to be in mechanical equilibrium within the trapped cloud we have

$$T\nabla n(\mathbf{r}) = (\mathbf{F}_A + \mathbf{F}_R - k\mathbf{r})n(\mathbf{r}). \tag{12}$$

For the special case $\mathbf{F}_A + \mathbf{F}_R - k\mathbf{r} = 0$ the density within the cloud is a constant, and we obtain Eq. (11). Taking the divergence of Eq. (12) and using Eqs. (4), (8), and (11) gives

$$T\nabla^2 \ln[n(\mathbf{r})] = 3k(n/n_{\max} - 1). \tag{13}$$

We may then numerically integrate Eq. (13) for a cloud of N atoms to find the spatial distribution of the atoms.

For the calculation of the spatial distribution of the atoms in the cloud, we assumed strong damping, no convective motions, and no temperature gradients. We also ignored the standing-wave patterns of the lasers (except in the averaging for $\langle\sigma_F\rangle$ and $\langle\sigma_L\rangle$ as discussed below) and the spatial profiles of the lasers. We emphasize that we are not claiming *a priori* that these and other complications discussed below should (or should not) be significant. We are simply presenting a model that is made tractable by the neglect of them and then showing the successes (and failures) of this model in its explanation of the observations.

The next stage of the calculation is to find $\langle\sigma_F\rangle$ and $\langle\sigma_L\rangle$ for the atoms in a laser field produced by three intersecting beams. The combination of beams creates a three-dimensional standing-wave field

$$I(x,y,z) = 6I_\infty \cos^2\left(\frac{2\pi x}{\lambda} + \frac{2\pi y}{\lambda} + \frac{2\pi z}{\lambda} + \phi\right), \tag{14}$$

where ϕ is an arbitrary phase factor. We may visualize this expression for the intensity by first considering the result of two counterpropagating beams of opposite circular polarization. This results in a local linear polarization that traces out a helix in space. Equation (14) follows, then, if we add the light from the two other directions. We obtain the spatially averaged cross section $\langle\sigma_L\rangle$ by averaging the cross section $\sigma_L = \sigma_0[1 + I(x,y,z)/I_S + 4(\Delta/\Delta_N)^2]^{-1}$ over a wavelength in an arbitrary direction, where σ_0 is the unsaturated, resonant cross section, I_S is the saturation intensity, $\Delta = \omega_L - \omega_0$ is the trap laser detuning, and Δ_N is the natural linewidth of the transition. We find that

$$\langle\sigma_L\rangle = \sigma_0\left\{\left[1 + 4\left(\frac{\Delta}{\Delta_N}\right)^2\right]\left[1 + \frac{6I_\infty}{I_S} + 4\left(\frac{\Delta}{\Delta_N}\right)^2\right]\right\}^{-1/2}. \tag{15}$$

We used this spatially averaged cross section, since this was the approach used in the calculation of $\langle\sigma_F\rangle$ in Ref. 9. Note that there are other effects that are, in principle, important in calculating $\langle\sigma_F\rangle$ and $\langle\sigma_L\rangle$, but we neglected them in the spirit of simplification discussed above. These include magnetic field and Doppler shifts, the polarization and coherence properties of the light, local optical pumping of the atoms, and Zeeman precession of the atoms in the magnetic fields.

The spatially averaged cross section $\langle\sigma_F\rangle$ for absorption of the reradiated light is different, in general, from that for the incident laser light, $\langle\sigma_L\rangle$. This is due to a change in the frequency properties of the scattered light produced by the ac Stark effect[9] (in our experiments the average light intensity is 6–12 times the saturation intensity). Calculating $\langle\sigma_F\rangle/\langle\sigma_L\rangle$ exactly is difficult for optically trapped cesium because of the many levels involved, each of which is shifted by the light field. For the purposes of this work we crudely estimated $\langle\sigma_F\rangle/\langle\sigma_L\rangle$, using the emission and absorption spectra for a two-level atom in a monochromatic one-dimensional standing-wave field. These spectra are illustrated in Fig. 3. The scattered-radiation spectrum contains an elastic component at the frequency of the incident photons and an inelastic component, which is the result of the ac Stark shift by the time-

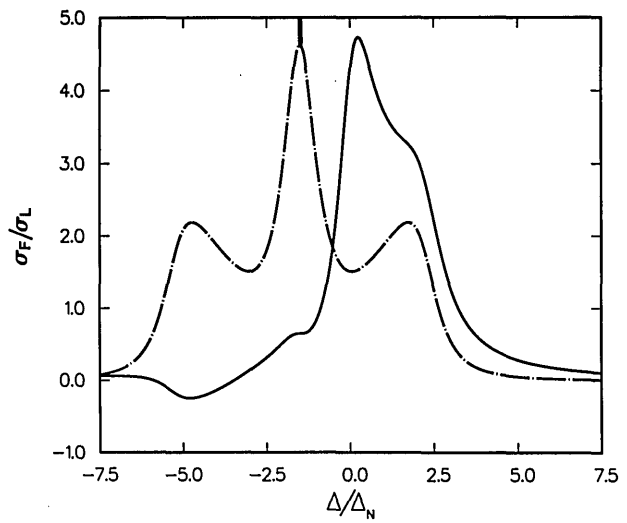

Fig. 3. Absorption (solid curve) and emission (dotted–dashed curve) profiles calculated for a two-level atom in a one-dimensional standing-wave field. The curves are for an average intensity of 12 mW/cm^2 and a laser detuning of $-1.5\Delta_N$. The emission profile is in arbitrary units. The zero-width elastic emission peak (which constitutes 50% of the total) is represented by the spike at $-1.5\Delta_N$.

dependent fields. This gives the familiar Mollow triplet for the emitted light. The absorption profile is strongly peaked near the blue component of this Mollow triplet. This causes the average absorption cross section for the emitted light, $\langle\sigma_F\rangle$, to be greater than that for the incident light, $\langle\sigma_L\rangle$; this critical difference is what causes the combination of attenuation and radiation trapping forces to give a net repulsive force between the atoms. Taking the convolution of the emission and absorption spectra in Fig. 3 to calculate $\langle\sigma_F\rangle$, we find that $\langle\sigma_F\rangle/\langle\sigma_L\rangle = 1.2$ for our experimental parameters (a detuning of $-1.5\Delta_N$ and a total average intensity $6I_\infty = 12$ mW/cm^2, where $\Delta_N =$ 5 MHz is the natural linewidth). Because $\langle\sigma_F\rangle > \langle\sigma_L\rangle$, Eq. (11) applies, and we expect the maximum density to be limited to $n < n_{max}$. We emphasize that although a number of approximations and simplifications were made in the calculation of $\langle\sigma_F\rangle$ and $\langle\sigma_L\rangle$, the basic physics of the expansion of the cloud relies only on the relation $\langle\sigma_F\rangle > \langle\sigma_L\rangle$. As long as the approximations do not change this relation, the cloud expands, subject to a maximum density given by Eq. (11).

B. Formation of Stable Orbits

The discussion in Subsection 2.A is valid for any number of atoms as long as the optical thickness is small and the pairs of trapping beams are exactly overlapping. However, a misalignment of the retroreflected trapping beams can put a torque on the cloud of atoms. As Subsection 4.D describes, we observe abrupt transitions to orbiting rings of atoms surrounding a central nucleus when the number of atoms exceeds a critical value. The formation of the stable orbits can be most easily understood by a consideration of the motion of atoms in the presence of a misalignment of the laser beams in the x–y plane (Fig. 4). Such a misalignment produces a local imbalance between the beams, and thus a force that may be represented phenomenologically by $\mathbf{F}_I = k'\hat{z} \times \mathbf{r}$. The optical trap also provides a restoring force $-k\mathbf{r}$ and a damping force $-\gamma d\mathbf{r}/dt$. Note that the tangential force $k'\hat{z} \times \mathbf{r}$ plus the damping force leads to a net orbital drift velocity. The existence of a small ball of atoms within the rings (Fig. 1) suggests that a force $(\alpha\eta_c N/r^2)\hat{r}$ due to radiation pressure from a central cloud of $\eta_c N$ atoms needs to be added as well as a radiation pressure force $[\alpha\eta_r N \ln(2\eta_r N/\pi)/2\pi r^2]\hat{r}$ on an atom in the ring due to the $\eta_r N$ other atoms in the ring ($\alpha = \langle\sigma_L\rangle\langle\sigma_F\rangle I/4\pi c$). Adding these, we obtain the equation of motion for the trapped atom:

$$m\frac{d^2\mathbf{r}}{dt^2} = -k\mathbf{r} - \gamma\frac{d\mathbf{r}}{dt} - k'\hat{z} \times \mathbf{r} + \frac{\alpha N'}{r_2}\hat{r}. \tag{16}$$

Here N' is the effective number of atoms that provide a repulsive radiation rapping force on the atom and is given by

$$N' = N\left[\eta_c + \frac{\eta_r \ln(2\eta_r N/\pi)}{2\pi}\right]. \tag{17}$$

In order to compare theory and experiment precisely, we must consider the spatial dependence of the trapping beams, which gives an $\mathbf{r}$ dependence to k, k', and γ. However, it is illustrative to ignore this spatial dependence for the moment so that Eq. (16) can be solved analytically. By trying the oscillatory solution $\mathbf{r} = R(\hat{x}\cos\omega t + \hat{y}\sin\omega t)$, we find that stable circular orbits exist at a radius

$$R = [\alpha N'/(k - m\omega^2)]^{1/3}, \tag{18}$$

with orbital frequency $\omega = k'/\gamma$. Thus we obtain orbital trajectories at a radius R as long as the condition $\omega < (k/m)^{1/2}$ is satisfied. This condition on the orbital frequency is violated if the torque on the cloud is too high or the damping is too small. In these cases the atoms fly out of the trap rather than orbit. Equation (18) shows that if the radiation pressure is increased (larger $\alpha N'$), the radius of the rings increases. The orbital radius also increases when the spring constant of the trap is decreased

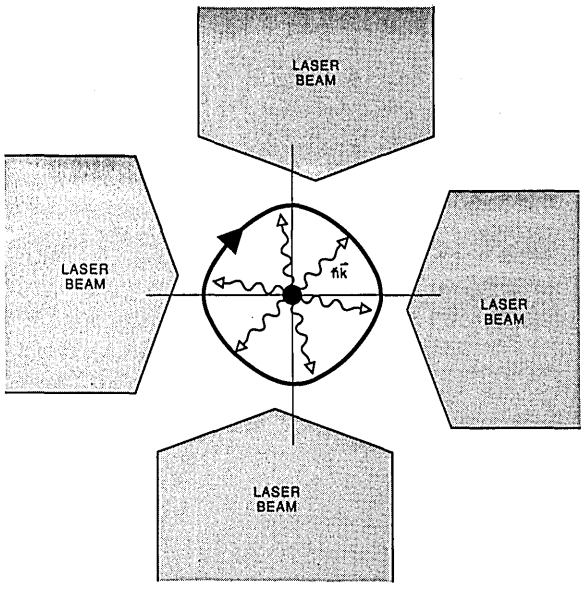

Fig. 4. Geometry of the misalignment in the horizontal plane that gives rise to the orbital modes. The bold boundary and the central ball show the positions of the atoms. The arrow indicates the direction of the orbit. The radiation pressure from the central core is also illustrated.

or the frequency of rotation increases. If the radiation pressure term is not included in Eq. (16), we find that there are no stable orbiting solutions.

We performed a more general calculation of the orbits than one would obtain by including the **r** dependence of k, k', and γ. Rather than using Eq. (16) to calculate this, it is more natural for one to consider the force due to four separate laser beams. We start by considering the spontaneous force $F_{X_\pm}$ on an atom for a single beam propagating in the positive or negative x direction, where the Gaussian shape of the beams, the saturation effects, the Zeeman shifts, and the Doppler shifts are included. This force is assumed to be given by

$$F_{X_\pm} = \frac{\pi h \Delta_N}{\lambda} \frac{\dfrac{I_\pm(y)}{I_S}}{1 + \dfrac{I(\mathbf{r})}{I_S} + \dfrac{4(\Delta \pm \omega_B' x \pm v_X/\lambda)^2}{\Delta_N{}^2}}, \tag{19}$$

where I_S is the saturation intensity ($I_S = 1$ mW/cm^2), $I(\mathbf{r})$ is the total local laser intensity, $\Delta = \omega_L - \omega_0$ is the detuning of the laser from line center, ω_B' is the Zeeman shift in frequency per unit length, and λ is the wavelength of the light. This equation for the force is what one obtains for a two-level atom, adding an *ad hoc* Zeeman shift and assuming that the intensities can be summed to determine the saturation. Although this assumed form is not exactly correct, we believe that it is a good approximation, which contains the relevant physics. The Gaussian intensity profile for the laser beams propagating in the $\pm x$ direction is given by

$$I_\pm(y) = I_\infty \exp\left\{-\left[\frac{2(y \mp s/2)}{w}\right]^2 \ln 2\right\} \equiv I_\infty g_\pm, \tag{20}$$

where s is the displacement of the beams with respect to each other and w is the full width at half-maximum (FWHM) of the Gaussian beam profile. By summing the forces in the forward and reverse directions and adding a radiation trapping force

$$F_{R_X} = \alpha N' x/(x^2 + y^2)^{3/2}, \tag{21}$$

we obtain a net force

$$F_X = F_{R_X} + \frac{\pi h \Delta_N I_\infty}{\lambda I_S} \times \frac{(g_+ - g_-)\left\{1 + \dfrac{I(\mathbf{r})}{I_S} + \dfrac{4[\Delta^2 + (\omega_B' x + v_X/\lambda)^2]}{\Delta_N{}^2}\right\} + (g_+ + g_-)\dfrac{\Delta(\omega_B' x + v_X/\lambda)}{\Delta_N{}^2}}{\left\{1 + \dfrac{I(\mathbf{r})}{I_S} + \dfrac{4[\Delta^2 + (\omega_B' x + v_X/\lambda)^2]}{\Delta_N{}^2} - \dfrac{64\Delta^2(\omega_B' x + v_X/\lambda)^2}{\Delta_N{}^4}\right\}^2}. \tag{22}$$

The total force on the atom is found by adding the forces in the x and y directions and is thus

$$\mathbf{F} = F_X \hat{x} + F_Y \hat{y}, \tag{23}$$

where F_Y is given by the transposition of x and y and the substitution of v_Y for v_X in Eqs. (21) and (22). These equations of motion for a single atom are solved numerically for the conditions $\Delta = -1.5\Delta_N$, $I(\mathbf{r}) = 12$ mW/cm^2, and $s = 1.5$ mm. The value of $\omega_B' = d\omega_B/dr$ is difficult to calculate, since the atoms are distributed among the various m levels. However, from our measurements of the spring constant and using the correct limits in Eq. (22), we derive a value of $\omega_B' = 10$ MHz/cm.

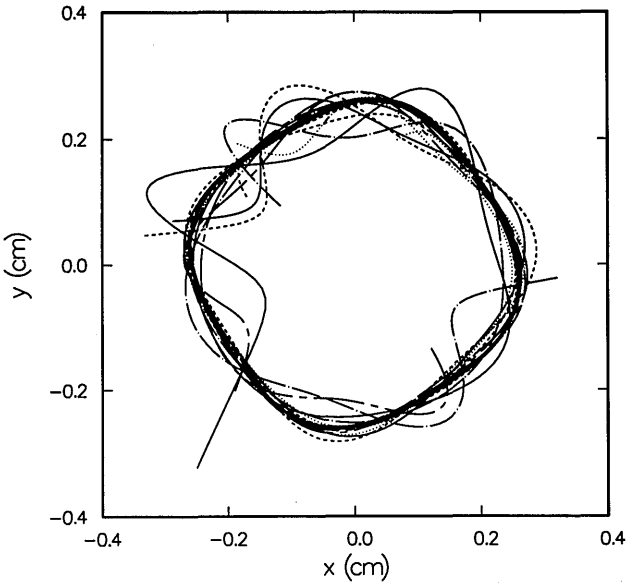

Fig. 5. Trajectories of an atom numerically calculated from our model. The trajectories are shown for ten initial positions and velocities of the atom. The trap parameters were chosen to be the same as for the conditions in Fig. 1(e) ($\Delta = -1.5\Delta_N$, $I/I_S = 12$, $B' = 15$ G/cm, $w = 6$ mm, and $s = 1.5$ mm). The frequency of the orbit is 82 Hz.

We first numerically solve the equations of motion for a radiation trapping force corresponding to an effective number of atoms, $N' \approx 5 \times 10^7$. Figure 5 shows the solutions to the equations of motion for several arbitrary starting positions and velocities of the atoms. The model is seen to predict that the atoms orbit in a ring that closely resembles the photographs in Fig. 1. The orbit has a mean radius of 2.5 mm and a rotational frequency of 82 Hz. For $N' \approx 9 \times 10^7$ the equations of motion predict that the atoms slowly spiral out of the trap, and for larger N' the atoms are rapidly ejected from the trap. If we examine the case of no radiation trapping force ($N' = 0$), we find that the atoms spiral into the center of the trap. Thus the radiation trapping force is necessary to an explanation of the existence of the orbits.

3. EXPERIMENTAL APPARATUS

To produce a cloud of trapped cesium atoms, we started with a thermal atomic beam with an average velocity of 250 m/s. These atoms were slowed to a few meters per second by counterpropagating laser light. The slowly moving atoms then drifted into the spontaneous force Zeeman-shift trap described below and were held there for times on the order of 100 s. The trap cooled the atoms so that their average velocity was approximately 20 cm/s in the nonorbiting mode and compressed the atoms to densities of as much as 10^{11} cm^{-3}. We studied the cloud of trapped atoms by observing the total fluorescence with a

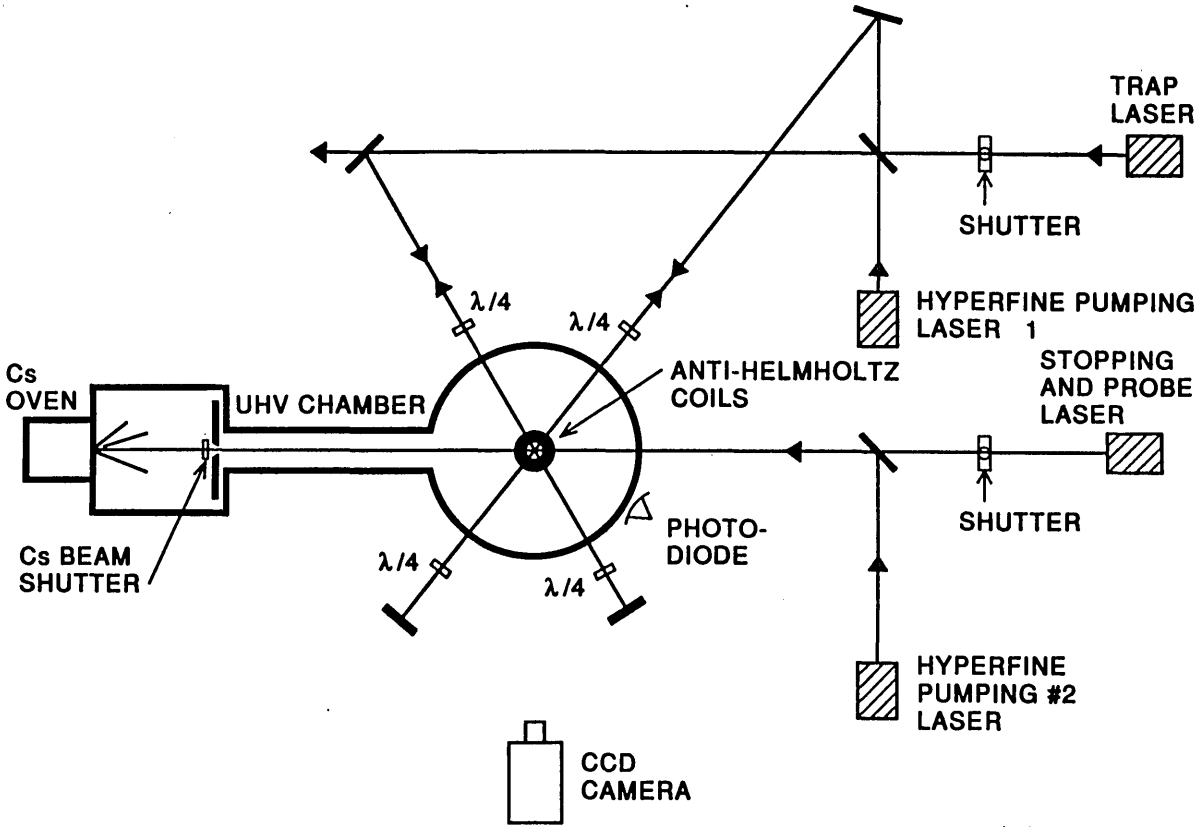

Fig. 6. Schematic of the experimental apparatus. The third trapping beam, perpendicular to the page, is not shown.

photodiode and the spatial distribution of the fluorescence with a calibrated charge-coupled device camera.

A schematic of the experimental apparatus is shown in Fig. 6. A beam of cesium atoms effused from an oven at one end of the vacuum chamber. A capillary array was used as an output nozzle for the oven to create a large flux of cesium atoms.[10] These atoms were then slowed by a frequency-chirped diode laser entering from the opposite (trap) end of the chamber. The distance from the oven to the trap was approximately 90 cm. This stopping laser drove the $6S_{1/2,F=4} \rightarrow 6P_{3/2,F=5}$ resonance transition. A second laser beam, which overlapped the first, excited the $6S_{1/2,F=3} \rightarrow 6P_{3/2,F=4}$ transition to ensure that atoms were not lost to the $F = 3$ ground state. The frequencies of these two lasers were swept from 500 MHz below the atomic transition to within a few megahertz of the transition in approximately 15 ms. At the end of each chirp the stopping laser was quickly shifted out of resonance, and the $F = 3$ state depletion laser remained at the same frequency that it had possessed at the end of the ramp. It took atoms 35 ms after the end of the chirp to drift into the trap, after which the 15-ms cooling chirp was repeated. The frequency of the stopping laser at the end of the chirp determined the final drift velocity of the atoms. The number of atoms loaded per chirp was largest when the velocity was approximately 8 m/s. We were able to load approximately 2×10^6 atoms per chirp into the trap under these conditions. The total number of atoms in the trap was determined by the balance between the loading rate and the collisional loss rate. When no loading was desired, shutters blocked the cesium and stopping laser beams.

The trap was similar to that described in Refs. 1 and 2. The trapping light was produced by a third diode laser tuned below the $6S_{1/2,F=4} \rightarrow 6P_{3/2,F=5}$ resonance transition. Data were taken over the range of detunings from 5 to 15 MHz. The output from this laser was passed through an optical isolator and was spatially filtered. It was then carefully collimated and split into three circularly polarized beams of 6-mm diameter (Gaussian half-power widths). These intersected orthogonally at the center of a pair of anti-Helmholtz coils with a 25-mm radius and a 32-mm separation. The beams were then reflected on themselves with the opposite polarization. The magnetic field produced by the coils was 0 at the center of the trap and had a vertical field gradient (5–20 G/cm) two times larger than the horizontal field gradient. The center of the trap was positioned 1 cm below the stopping laser so that the slowing process would not eject the previously trapped atoms. A fourth laser tuned to the $6S_{1/2,F=3} \rightarrow 6P_{3/2,F=4}$ transition pumped atoms out of the $F = 3$ ground state in the trap.

All lasers used in this experiment were stabilized diode lasers with long-term stabilities and linewidths of well under 1 MHz. We frequency-stabilized the stopping and trapping lasers by optically locking them to an interferometer cavity.[11] This was done by our sending approximately 10% of the laser light to a 5-cm Fabry–Perot interferometer located a few centimeters from the laser. The cavity was tilted slightly so that the beam entered at an angle relative to the cavity axis. The cavity returned of the order of 1% of this light to the laser and caused the laser to lock to the resonant frequency of the cavity. The two other lasers, which were used for hyperfine pumping,

were stabilized by feeding back light from a grating in the Littrow configuration. The front surface of these laser diodes was antireflection coated so that the grating served as a tuning element for the laser frequency and as one of the end mirrors of the laser cavity. The frequencies of all four lasers were monitored with small cesium saturated-absorption spectrometers. The absorption signals were used to derive error signals, which were fed back electronically to control the laser frequencies by changing the laser currents and/or cavity lengths.

In this experiment we observed that the shape and the density of the cloud of atoms depended sensitively on the alignment of the trapping beams. We had also discovered, in a previous experiment[5] on collisional loss of atoms from the trap, that the depth of the trap was sensitive to the alignment. For a reproducible experiment, we found that care must be taken to obtain a symmetric trapping potential. We could obtain consistent results only if we carefully centered all the spatially filtered trapping beams on the magnetic field zero while the vacuum chamber was open. In addition, the Earth's magnetic field was zeroed to 0.01 G so that the field gradient of the trap was radially symmetric. Before these precautions were taken, we observed a large variety of density variations and unpredictable cloud shapes within the trap. We note that motions of atoms in traps with misalignment were briefly described in Ref. 2, but it is difficult to compare our results with those because of the brevity of that discussion.

4. RESULTS

We now discuss our experimental observations and compare them with our models. First we determined the shape of the trap potential and measured the temperature of the trapped atoms. We then measured the dependence of the cloud shape and size on the number of atoms in the trap. Finally, we studied the atoms' behavior in the orbital mode. This included observing the shape of the orbits, the orbital frequencies, and the transitions between modes.

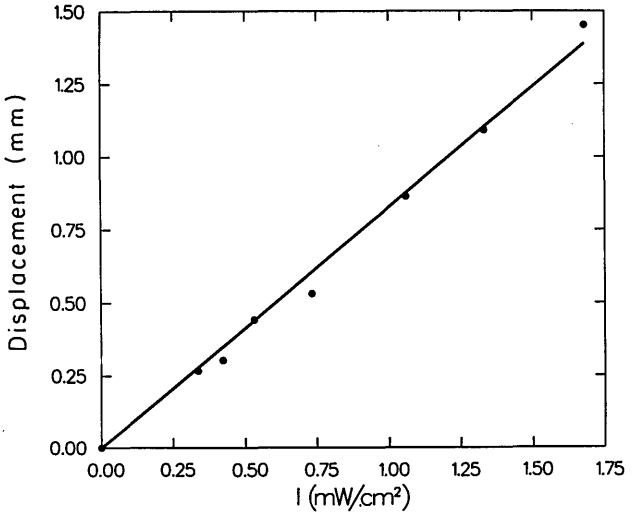

Fig. 7. Displacement of a small ball of atoms versus intensity of the pushing beam (circles). The solid-line fit shows that the force is harmonic and gives a spring constant of 6 K/cm^2. The laser detuning was $-1.5\Delta_N$, the total intensity was $I/I_S = 12$, and the magnetic field gradient was 15 G/cm. The pushing beam was at the same frequency as the trap laser.

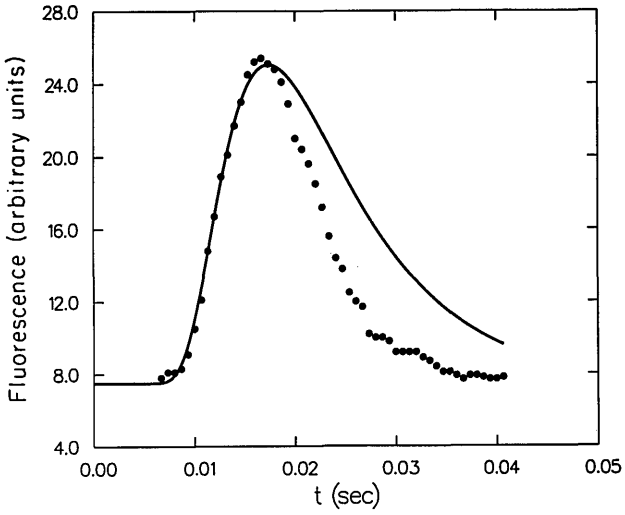

Fig. 8. The dots show the TOF spectrum, after the trap light is turned off and the fluorescence is measured, of a probe beam 4 mm to the side of the cloud. The solid curve is a fit to the data for a Maxwell–Boltzmann distribution (T = 265 μK) that heavily weights the rising edge of the TOF spectrum.

A. Trap Potential

We measured the trap potential by observing the displacement of a small ball of trapped atoms when they were pushed by an additional laser, as was done in Ref. 2. This pushing laser was split off from the trapping laser beam and was linearly polarized. The plot of displacement versus pushing intensity is shown in Fig. 7. The fit indicates that the trap potential was harmonic out to a 1.5-mm radius. The spring constant was 6 K/cm^2 for a detuning of $-1.5\Delta_N$ and a magnetic field gradient of 15 G/cm. We were unable to measure the trap potential beyond 1.5 mm because at larger radii it was difficult to displace the small ball of atoms in a line.

B. Temperature of Atoms

To measure the average temperature of the trapped atoms, we passed a 0.5-mm-diameter probe beam 4 mm from the side of the cloud. We then observed a time-of-flight (TOF) spectrum[12] after the trap light was rapidly shifted out of resonance. This shift effectively turns off the optical trap quickly, and we accomplished it by switching the current on the trapping laser so that the laser frequency was moved many gigahertz from the atomic transition. The switching time with this technique was well under 10 μs. Approximately 0.5 ms later, all the lasers, except for the probe laser and pumping laser 1, were mechanically shuttered to reduce the scattered light in the vacuum chamber. We then obtained the TOF spectrum from the fluorescence of the probe laser. Figure 8 shows the average of 16 TOF spectra.

In calculating the theoretical fit in Fig. 8, we assumed a Maxwell–Boltzmann distribution of velocities and heavily weighted the rising edge of the TOF spectrum. The fit gives a temperature of 265 μK for a cloud with approximately 5×10^6 atoms. The poor fit shows that either there is a spatially dependent temperature in the cloud or the velocity distribution is non-Maxwellian.

The plot of temperature (as defined by the above arbitrary procedure) versus cloud diameter is shown in Fig. 9(a) for two detunings. In both cases the tempera-

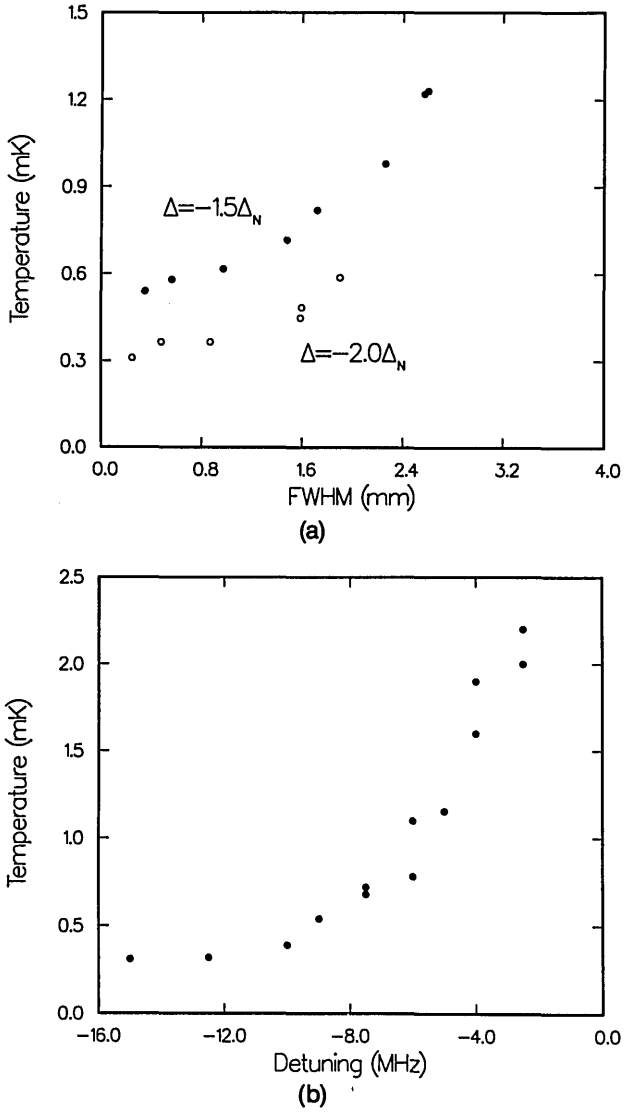

Fig. 9. Measured temperature of the atoms versus the diameter (FWHM) of the cloud for detunings of $-1.5\Delta_N$ (filled circles) and $-2.5\Delta_N$ (open circles). (b) Measured temperature of the atoms versus detuning for a 1.5-mm-diameter cloud. The total laser intensity is 12 mW/cm^2, and the magnetic field gradient is 15 G/cm.

ture increases with increasing numbers of trapped atoms. We speculate that this heating arises from radiation trapping. From Fig. 3 we note that since the blue-shifted light is preferentially absorbed, the light that escapes the cloud is red shifted on average from the incident trapping light. The excess energy may then be converted to kinetic energy of the atoms. We did not investigate in detail how this occurs.

Figure 9(b) shows the plot of measured temperature versus detuning for clouds of a fixed diameter (1.5 mm). No significant temperature changes were observed when the magnetic field gradient was changed or when the intensities of the lasers were changed.

We emphasize that, although the temperature rises with increasing numbers of atoms, the temperature rise would need to be orders of magnitude larger to explain the observed expansion of the cloud.

C. Dependence of Cloud Shape on Number of Atoms

Three well-defined spatial modes of the trapped atoms were observed. These depended on the number of atoms in the trap and on how the trapping beams were aligned. These modes are described in detail here and in Subsection 4.D.

The ideal-gas mode occurred when the number of atoms was fewer than approximately 80,000. The atoms formed a small sphere with a diameter of approximately 0.2 mm. We found the distribution of the atoms by digitizing the image of the cloud and assuming that the observed light intensity was directly proportional to the number of atoms along the line of sight. The density distribution of the atoms is shown in Fig. 10(a) and clearly matches the Gaussian dependence that one would expect for an ideal gas in a harmonic potential. The density increase was proportional to the number of atoms as atoms were added, but the diameter remained unchanged. Using the measured spring constant, we derived a temperature from the fit to the distribution. We found a temperature of 300 μK for the atoms, which agrees well with the TOF temperature measurement.

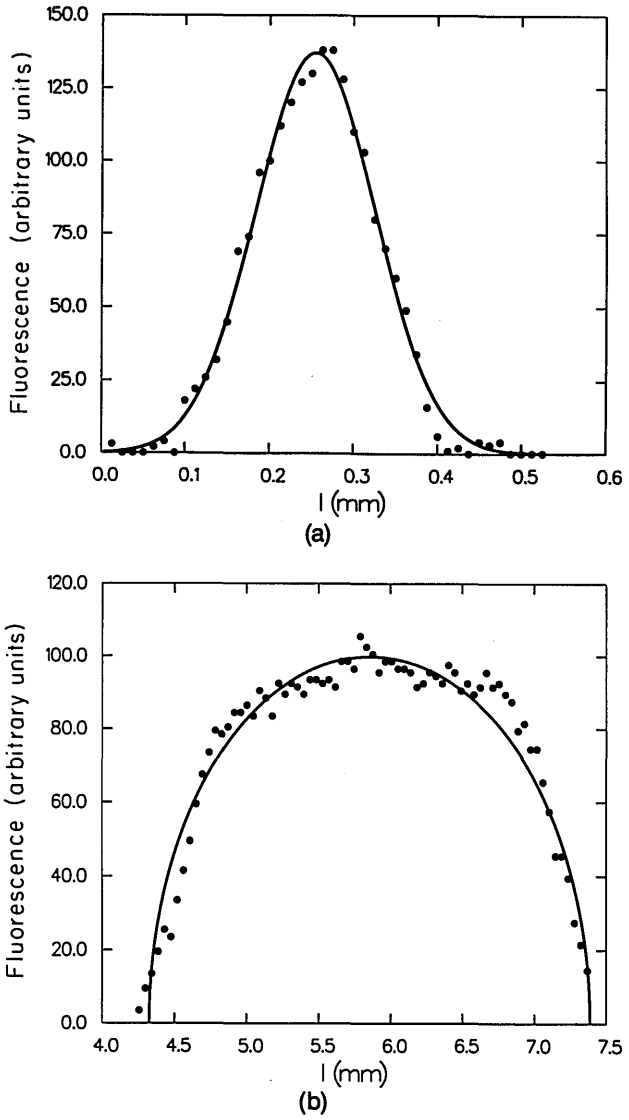

Fig. 10. Top view of fluorescence profile of the cloud. (a) Data for the ideal-gas mode (circles) with a fit (solid curve) for a Gaussian distribution. (b) Data for the static mode (circles) with a fit (solid curve) assuming that we are looking along the minor axis of a ellipsoid of constant density. The fit gives a ratio of 1.5 for the ellipsoidal axes.

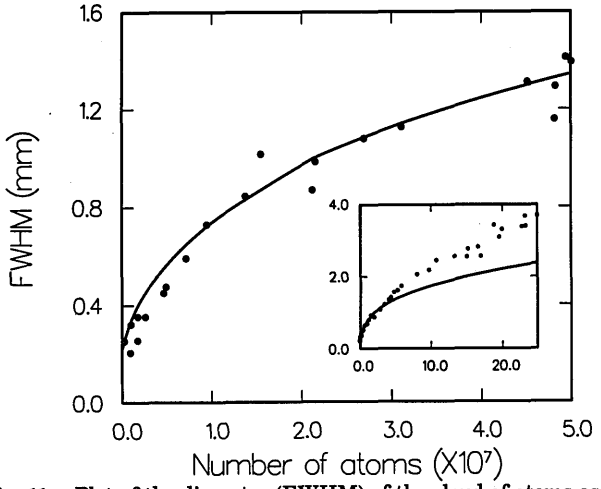

Fig. 11. Plot of the diameter (FWHM) of the cloud of atoms as a function of the number of atoms in the cloud (circles). For the main figure the magnetic field gradient is 9 G/cm, and for the inset it is 16.5 G/cm. The laser detuning is $-1.5\Delta_N$, and the total laser intensity is 12 mW/cm^2. The solid curves show the predictions of the mode that are described in the text.

When the number of atoms was increased past 80,000, the cold atoms no longer behaved as an ideal gas and the presence of a strong long-range force was evident. This static mode was characterized by an elliptically symmetric cloud, the diameter of which increased with increasing numbers of atoms. One distinctive feature of this regime was that the density did not increase as we added more atoms to the trap. Instead of following the Gaussian distribution of the ideal-gas mode, the atoms were distributed fairly uniformly, as Fig. 10(b) illustrates. We obtained these data by looking through the cloud along the axis with the greater (2×) magnetic field gradient. The solid curve shows the calculated distribution of fluorescence for an ellipsoidal cloud of atoms with an aspect ratio of 1.5 and constant density. The cloud's minor axis was along the direction of the higher magnetic field gradient. By looking along a major axis, we found that the aspect ratio varied from approximately 1 for a 1-mm diameter (FWHM) cloud to 2 for a 4-mm cloud.

We studied the growth of the cloud by measuring the number of atoms versus the major-axis diameter of the cloud. We performed this measurement by filling the trap with as many atoms as possible and then turning off the loading. With a charge-coupled device camera we recorded the evolution of the fluorescence as the atoms were lost from the trap and stored this record on video tape. We calibrated the video signal by also measuring the total fluorescence with a photodiode. To analyze these data, we digitized the frames of the video and stored them for analysis. We determined the total fluorescence in each image to obtain the number of atoms, and we calculated the FWHM diameter of the image. The results are shown in Fig. 11. Note that if the cloud were an ideal gas, the temperature would have to be of the order of 50 mK to explain the cloud's expansion. This supports our earlier claim that the expansion is not due to a rise in temperature.

We obtained the fit (solid curve) to the data (circles) in Fig. 11 by integrating Eq. (13), given N atoms, to predict the FWHM diameter of the cloud. We assumed the temperature dependence shown in Fig. 9(a) for a detuning of $-1.5\Delta_N$, but the results are insensitive to this parameter. The only free parameter in this calculation is the ratio $\langle\sigma_F\rangle/\langle\sigma_L\rangle$. A value of $\langle\sigma_F\rangle/\langle\sigma_L\rangle = 1.3$ gives the solid curve shown in Fig. 11. This is greater than the value of $\langle\sigma_F\rangle/\langle\sigma_L\rangle = 1.2$ given by the theory, discussed in Section 2, for a two-level atom in a one-dimensional standing-wave field. However, it is not surprising that our cesium atoms with 20 relevant levels in a three-dimensional field differed from the two-level case by this amount. The inset of Fig. 11 shows that our theoretical model for the expansion of the cloud deviates from the data at diameters greater than 1.5 mm. In fact, these data show that the density reached a maximum and then started to decrease as we added more atoms. However, the assumption of a harmonic potential may break down in this regime. Also, the cloud stability at such large sizes was quite sensitive to the alignment and the spatial quality of the trapping beams. Other effects that are not considered in this model but that may be important for clouds of this size are magnetic field broadening, multiple levels of the atom, polarization of the scattered light, and multiple (>2) scattering of the light. Taking these effects into account makes the equation of equilibrium for large clouds quite complex.

We were able to obtain as many as 4×10^8 trapped atoms in this static mode if the trapping laser beams were retroreflected (<1 mrad). However, if the return beams were slightly misaligned in the horizontal plane, dramatic and abrupt transitions to orbiting clumps or rings occurred at approximately 10^8 atoms.

D. Rotating Clumps and Rings

We now describe the observed spatial distributions and orbital motions for the third mode of the trapped atoms, which we call the orbital mode. This mode is characterized by atoms orbiting a central ball and abrupt transitions between different orbital modes and between static and orbital modes. We studied how the atoms' motion depends on a variety of parameters. Here we compare the data with the numerical model described above. This model explains much of the equilibrium behavior; however, it does not explain the clumping or any of the transition dynamics that are observed.[13]

Photographs of the orbital modes are shown in Fig. 1 [Figs. 1(b)–1(e) show the top view, and Fig. 1(f) shows the side view]. We first observed a ring surrounding a dense central ball of atoms (henceforth known as the nucleus), as Fig. 1(b) shows. By strobing the camera, we then found that the ring was actually a clump of atoms rotating counterclockwise around the nucleus, as Fig. 1(c) shows. Note that there is a tenuous connection between the nucleus and the clump and that the nucleus has an asymmetry that rotates with the clump. The orbital radius of these clumps was insensitive to the trapping laser intensity, the detuning, and the magnetic field gradient. The rotational frequency did depend on these parameters, which we discuss below. We also observed clumps rotating at smaller radii, as Fig. 1(d) shows. These smaller orbits occurred when fewer atoms were in the trap. The rotating clump had as many as three different radii with abrupt transitions between them as the number of atoms changed. The different orbital radii depended on the number of trapped atoms and varied in size by a factor of 3. Within each of the intermediate stages the radius of the orbit slowly increased as we added more atoms until

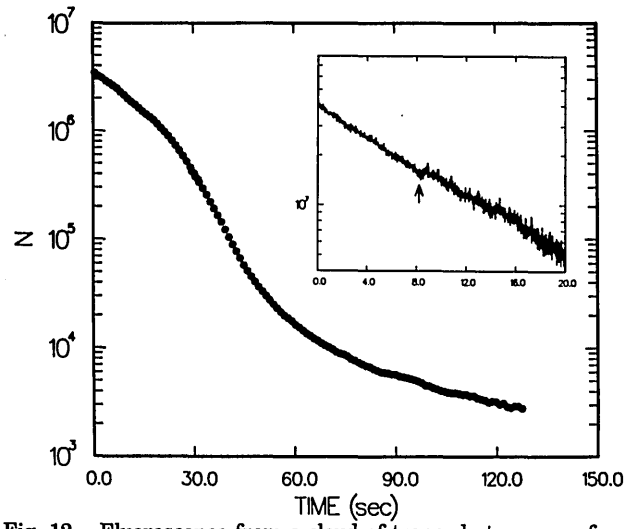

Fig. 12. Fluorescence from a cloud of trapped atoms as a function of time after the loading is terminated. The main figure shows the decay of atoms from the static mode into the ideal-gas mode. The inset shows the decay from an orbiting mode through an abrupt transition (indicated by the arrow) to the static mode.

the cloud suddenly jumped to the next stage. The rotating clump in these intermediate stages was not so extended as it was for the larger radii shown in Fig. 1(c), and there was a large number of atoms connecting the clump to the nucleus. The size of the clump took up approximately one quarter of the area shown in the unstrobed image.

Another orbital shape that we observed was a continuous ring surrounding a nucleus [Fig. 1(e)]. We assumed that the atoms were still orbiting in this mode but that no clumping of the atoms occurred. Unlike in the rotating clump case, the radius of the continuous ring increased by a factor of 2 as we increased the detuning or decreased the magnetic field gradient. The rectangular shape of the ring was formed by the intersection geometry of the laser beams, with the corners of the ring corresponding to the centers of the beams. The atoms lay in a horizontal plane approximately 0.5 mm thick [Fig. 1(f)]. Approximately 80% of the atoms were in the outer ring, with the remaining 20% contained in the nucleus.

The formation of these orbital modes depended critically on the alignment of the trapping beams in the horizontal plane. The beams had a Gaussian width of 6 mm, and the return beams were misaligned horizontally by 4–8 mrad (1–2 mm) at the trap region. It was observed that the direction of rotation corresponded to the torque produced by the misalignment (Fig. 4). If the vertical trapping beam was misaligned, the plane of the rotation could be tilted by as much as 20°, but no stable orbits were observed in the vertical direction. We believe that this was due to an asymmetry in the trapping force caused by the vertical magnetic field gradient's being two times larger than that of the horizontal. The shape of the rings depended on the alignment and could be changed by tilting the retroreflection mirrors. The rings had stable orbits at radii from 2 to 3 mm. No rings were observed at radii < 2 mm. At radii > 3 mm the ring would form for only a few tenths of a second, then become unstable, and the atoms would fly out of the trap.

The degree of misalignment in the horizontal plane and the number of atoms determined which of the orbital modes occurred. When enough atoms were loaded into the trap, the cloud typically switched into the rotating clump for misalignments between 4 and 6 mrad and into the continuous ring for those between 6 and 8 mrad. If the light beams were misaligned even further, the atoms continuously loaded into the ring mode for any number of atoms, and for large misalignments we could even form a ring with no visible nucleus. In Ref. 3 we reported that a nucleus of atoms always exists, but we can now make rings without nuclei by a suitable adjustment of the various trap parameters.

We also studied how the trap loss rate depended on the mode. This was done by observation of the time evolution of the cloud when no additional atoms were being loaded. Another study of interest was to see how long various cloud modes survived as the number of atoms decreased owing to atomic collisions. These data are shown in Fig. 12. The total fluorescence from the cloud, which we assumed to be proportional to the number of atoms, indicates that there were initially 4×10^7 atoms in the orbital mode (inset of Fig. 12) and that the fluorescence decreased exponentially with a time constant of $\tau \approx 9$ s. With 1.5×10^7 atoms remaining, the cloud abruptly jumped into the static mode, and the number of atoms continued to decrease exponentially with time ($\tau \approx 10$ s). This transition is indicated by the arrow in the figure. The main plot in Fig. 12 shows a decay of fluorescence from a different run starting with 4×10^6 atoms in the static mode. In this run the initial time constant was approximately 17 s rather than the 10 s shown in the inset, owing to a lower vacuum pressure in the chamber. As the cloud started to change from the static mode to the ideal-gas mode after approximately 30 s, the loss rate increased. We believe that this was due to an increase in losses resulting from collisions between the trapped atoms, as Ref. 4 describes. At this point the density had reached its maximum value. Finally, after so many atoms were lost that the density was much lower ($\approx$70 s), the fluorescence decayed with a time constant of $\tau \approx 60$ s. This loss rate was due entirely to the collisions with the 2×10^{-10} Torr of background gas in the vacuum chamber.

The rotational frequencies of the clumps were monitored either by strobing the image viewed by the camera or by observing the sinusoidal modulation of the fluorescence by a photodiode [Fig. 13(a)]. The peak-to-peak amplitude of this modulation was from 10% to 50% of the total fluorescence. Although it is obvious that the fluorescence from a limited portion of the orbit should vary, it is somewhat surprising that the total fluorescence should show such large modulations. The frequencies of rotation were between 80 and 130 Hz for the larger radii as we changed the trap parameters and were approximately 15% higher for the smaller orbits. As Fig. 14 shows, the orbital frequency depended on the detuning of the trapping laser (Δ), the magnetic field gradient (B'), and the intensity of the trapping light (I). Changing any of these parameters so as to increase the spring constant of the trap caused the rotation frequency to increase. The circles in Fig. 14 show the data points, and the pluses show the results of our model when we use Eq. (22). The experimentally observed orbital radius varied by less than 10% over the range of detunings, magnetic field gradients, and intensities used. In the calculation of the frequency as

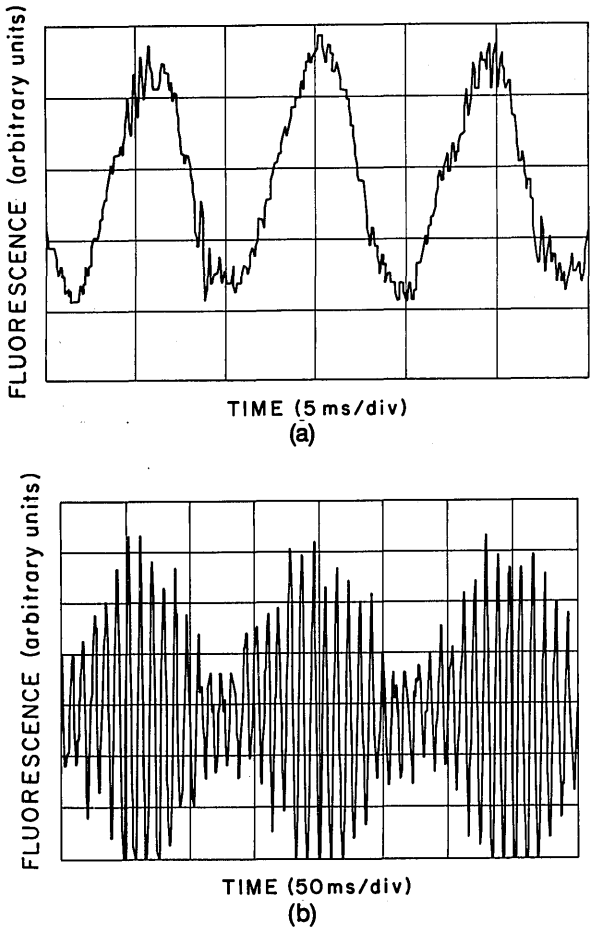

Fig. 13. (a) Time dependence of total fluorescence for the rotating clump without modulation of the magnetic field. (b) Beat signal of total fluorescence produced after the transition is induced to the rotating clump mode. The orbital frequency was 112 Hz, and the magnetic field was modulated at 119 Hz. The peak-to-peak modulation was approximately 40% of the total fluorescence for both (a) and (b).

a function of the magnetic field gradient and the laser intensity, the number of atoms composing the nucleus in our model was adjusted to keep the orbital radius constant because we saw no change in the experimental radius. The calculated radius had little sensitivity to the laser detuning, so that no adjustment was needed in the calculation of values of orbital frequency versus detuning. The calculated values show excellent agreement with all the experimental data, considering the simplicity of this model.

One of the notable features that this model does not explain is the observed abrupt transitions between modes. These transitions occurred when the number of atoms exceeded a particular critical value, and they lasted roughly 20 ms. The transition to the largest rotating clump mode involved usually several intermediate transitions to rotating clumps with smaller orbital radii, as we discussed above. In the case of the continuous ring the atoms always jumped directly into this mode from the static mode, with no intermediate stages.

We discovered that we could induce the transitions from the static mode to rotating clumps at fewer than the usual number of atoms ($\approx 10^8$) by modulating the magnetic field gradient at a frequency close (within 8 Hz) to the rotational frequency. In this case the number of atoms needed

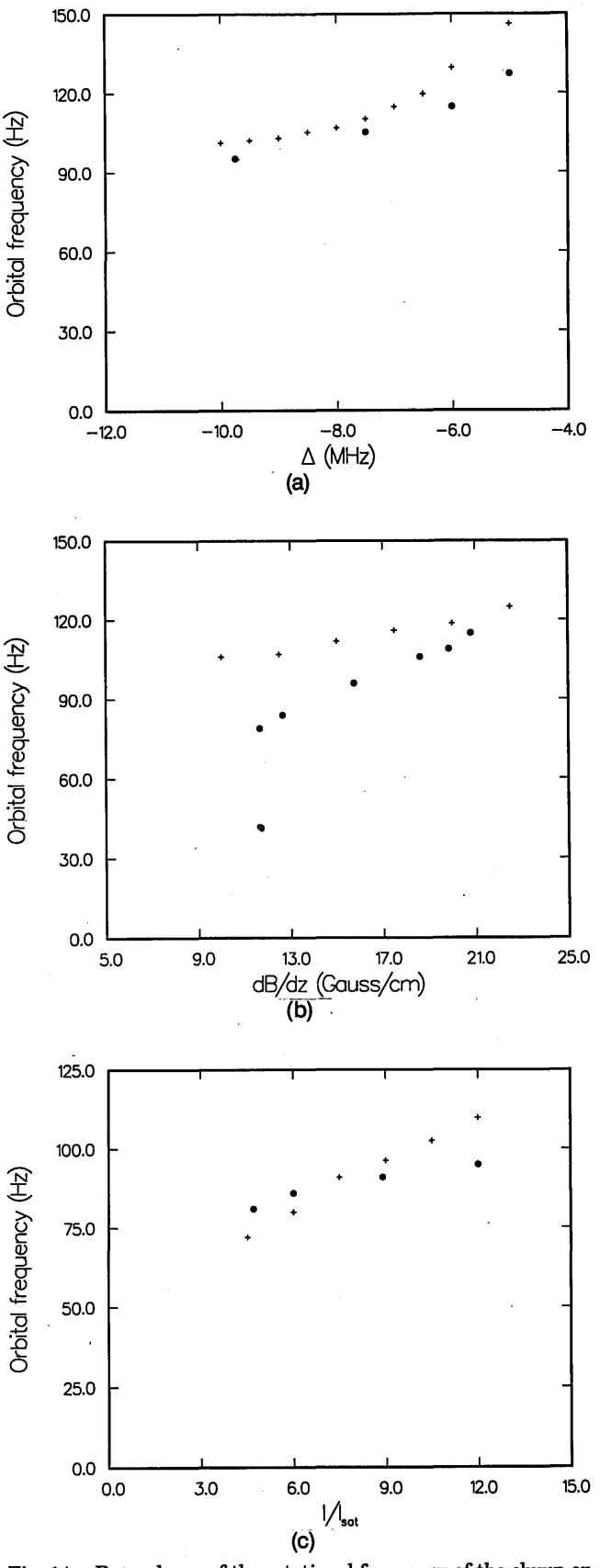

Fig. 14. Dependence of the rotational frequency of the clump on (a) the laser detuning ($B' = 12.5$ G/cm, $I = 12$ mW/cm^2), (b) the magnetic field gradient ($\Delta = -1.5\Delta_N$, $I = 12$ mW/cm^2), and (c) the total average intensity ($\Delta = -2.0\Delta_N$, $B' = 15$ G/cm). The circles are the experimental data, and the pluses give the results of our numerical model.

for the transition ($\approx 10^7$) depended on the amplitude and the detuning of the magnetic field modulation from the orbital resonance. Another amusing phenomenon was the following: after the cloud had made a transition, the fluorescence was modulated at the beat frequency between the two frequencies. This is shown in Fig. 13(b).

Profound hysteresis effects were observed in the transition between the static and the orbital modes. If the number of atoms was slowly increased to 10^8, the cloud suddenly jumped from the static mode to the rotating clump, and the trap lost approximately half of its atoms in the succeeding 50–100 msec. This orbital mode remained stable at 5×10^7 atoms until there was presumably a small fluctuation such as a change in the loading rate. Then the cloud switched back to the static mode without losing any atoms. It was necessary that the number of atoms build back up to 10^8 before it could again jump into the orbital mode. Thus the orbital modes can be self-sustaining at lower numbers of atoms than those required for a transition. This implies that when the atoms are in a different mode, the cloud obeys a different equation of equilibrium.

We occasionally observed a different hysteresis in the transition between the static and continuous ring orbital modes. The cycle started in the static mode with 10^8 atoms. Subsequently, 80% of these atoms jumped into a continuous ring, while 20% remained in the nucleus. In the succeeding couple of seconds most of the atoms in the ring transferred back into the nucleus. When this occurred, the nucleus grew in size and the radius of the ring decreased. Finally, with approximately 70% of the initial atoms back in the nucleus and 30% in the ring, the cloud collapsed back into the static mode. This transition occurred just before the outer diameter of the nucleus and the inner diameter of the ring merged. During this process the total number of atoms in the trap remained relatively constant. The cloud repeatedly switched between the two modes with an oscillation period of a few seconds.

In addition to the abrupt collective transitions there are a variety of other features of the orbital mode that cannot be described by the simple model. These include the clumping of the orbiting atoms, the number of atoms that appear in the core nucleus versus that in the ring, and the discrete radii of the clumps. The formation of clumps with discrete radii and the interesting transition dynamics may indicate the presence of some nonlinear interaction. A number of effects that we neglected could lead to such nonlinearities. For example, the radiation trapping and attenuation forces can change locally because of the local variation in the density or the polarization of the atoms. It is possible that this dependence of the equation of equilibrium on density could cause a rapid buildup of the number of orbiting atoms and also the forces keeping them there. The possible nonlinear processes inside a dense cloud of low-temperature atoms are not well understood and certainly deserve study.

5. CONCLUSION

We observed that the motions of atoms in a spontaneous force optical trap have an unexpectedly rich behavior. They act collectively at surprisingly low densities and make abrupt transitions. This behavior arises from the coupling between the atoms owing to the multiple scattering of photons and is enhanced by the change in the frequency properties of the scattered light. This force is a key element in the equation of equilibrium for optically trapped atoms and limits the obtainable density. A simple model was presented that explains the growth of the cloud and the formation of the circular rings. However, it does not give an explanation of the formation of the clumps or the dynamics of the transitions between different distributions.

ACKNOWLEDGMENTS

This work was supported by the U.S. Office of Naval Research and the National Science Foundation. We are pleased to acknowledge the valuable contributions made by C. Monroe and W. Swann to this work.

The authors are also with the Department of Physics, University of Colorado, Boulder, Colorado 80309-0440.

REFERENCES AND NOTES

1. D. Pritchard, E. Raab, V. Bagnato, C. Wieman, and R. Watts, Phys. Rev. Lett. **57,** 310 (1986).
2. E. L. Raab, M. G. Prentiss, A. E. Cable, S. Chu, and D. E. Pritchard, Phys. Rev. Lett. **59,** 2631 (1987).
3. T. Walker, D. Sesko, and C. Wieman, Phys. Rev. Lett. **64,** 408 (1990).
4. A. Gallagher and D. Pritchard, Phys. Rev. Lett. **63,** 957 (1989).
5. D. Sesko, T. Walker, C. Monroe, A. Gallagher, and C. Wieman, Phys. Rev. Lett. **63,** 961 (1989); M. Prentiss, A. Cable, J. Bjorkholm, S. Chu, E. Roab, and D. Pritchard, Opt. Lett. **13,** 452 (1988).
6. J. Dalibard, Opt. Commun. **68,** 203 (1988).
7. A. P. Kazantsev, G. I. Surdutovich, D. O. Chudesnikov, and V. P. Yakovlev, J. Opt. Soc. Am. B **6,** 2130 (1989).
8. L. D. Landau and E. M. Lifshitz, *Fluid Mechanics* (Pergamon, Oxford, 1989), p. 6.
9. B. R. Mollow, Phys. Rev. **188,** 1969 (1969); Phys. Rev. A **5,** 2217 (1972); D. A. Holm, M. Sargent III, and S. Stenholm, J. Opt. Soc. Am. B **2,** 1456 (1985).
10. S. Gilbert, Ph.D. dissertation (University of Michigan, Ann Arbor, Mich., 1984).
11. B. Dahamani, L. Hollberg, and R. Drullenger, Opt. Lett. **12,** 876 (1988).
12. P. D. Lett, R. N. Watts, C. I. Westbrook, W. D. Phillips, P. L. Gould, and H. J. Metcalf, Phys. Rev. Lett. **61,** 169 (1988); P. D. Lett, W. D. Phillips, S. L. Rolston, C. E. Tanner, R. N. Watts, and C. I. Westbrook, J. Opt. Soc. Am. B **6,** 2084 (1989).
13. R. Sinclair (Division of Physics, National Science Foundation, Washington, D.C. 20550, personal communication) has pointed out that the clumping is similar in character to the negative-mass instability that is observed in electron plasmas. We are now investigating this analogy.